

Analysis of Small-Aperture Radio-Frequency Pulsar Data

Ryan McKnight, Brian C. Peters, Zachary Arnett, Sabrina Ugazio *Ohio University*

BIOGRAPHY

Ryan McKnight is a Ph.D. candidate at the Avionics Engineering Center, School of Electrical Engineering and Computer Science, Ohio University, where he has worked on PNT research since 2017. His research interests include small satellites, GNSS interoperability, GNSS interference monitoring, weak-signal GNSS, pulsar-based navigation/timing, and deep space navigation. He was previously involved with the development and operations of the Bobcat-1 CubeSat. He received his M.S. in Electrical Engineering from Ohio University in 2023.

Brian C. Peters is pursuing his Ph.D. in Electrical Engineering and Computer Science at Ohio University as part of the Avionics Engineering Center. He completed his M.S. in Electrical Engineering at Ohio University in 2021 where he was involved with the development and operation of the Bobcat-1 CubeSat and conducted research on estimation of GNSS inter-constellation time offsets.

Zachary Arnett is pursuing his Ph.D. in Electrical Engineering and Computer Science at Ohio University as part of the Avionics Engineering Center. His research interests include GNSS inter-constellation time offset determination and radio-frequency pulsar navigation and timing. He received his M.S. in Electrical Engineering from Ohio University in 2023.

Sabrina Ugazio is an Assistant Professor at Ohio University. She obtained her Ph.D. in Electronics and Telecommunications at Politecnico di Torino (Italy) in 2013. Her research interests include timing, remote sensing, GNSS interoperability and space applications.

ABSTRACT

Pulsars have been known for more than half a century as possible time references which could also be used for navigation purposes. Both X-ray and radio-frequency (RF) signals have been considered for different applications. However, the use of pulsar signals has some practical challenges, mainly due to the low signal power. While X-ray systems may be bulky, complex, and expensive, RF systems may involve large antenna apertures or even longer observation times. However, modern technology such as powerful computation and storage capability as well as low noise RF amplification at accessible costs are making RF pulsar timing and navigation increasingly practical. The possible applications could be diverse. For example, several critical infrastructure applications, such as electrical power grids, require an accurate absolute timing reference, making apparent the need for backups to GNSS timing. On another hand, pulsar navigation could enable new opportunities for deep space applications, which is becoming increasingly relevant. The performance of a RF pulsar-based system for navigation and timing applications depends on a multitude of hardware and software parameters. In previous work (McKnight et al., 2022) the authors proposed and analyzed the preliminary design of a practical experiment to collect RF pulsar data and perform timing measurements. In this work, the data processing techniques needed for the experiment are developed, and the performance is evaluated using simulated data based on the proposed hardware design.

I. INTRODUCTION

Pulsars are rotating neutron stars that appear to a distant observer to emit a series of stable, regular pulses (Condon & Ransom, 2016). They were first discovered in 1967 by Jocelyn Bell at the Mullard Radio Astronomy Observatory in Cambridge, UK (Hewish et al., 1968). The pulsation effect is caused by the rapid rotation of the neutron star. The star emits a high-energy beam of electromagnetic radiation which is not necessarily aligned with its rotation axis. As it rotates, the beam sweeps through space and is observed at a distance as a series of regular, short pulses. To-date, over 2000 individual pulsars have been identified (Shemar et al., 2016), each with a unique pulsation period and profile determined by the characteristics of the neutron star. Typically, the rotational periods range from just a few milliseconds to several seconds. The stability of pulsar signals has been claimed to rival the stability of atomic clocks (Rawley et al., 1986), leading to the proposed use of these signals for a variety of applications. These include gravitational wave detection (Becker et al., 2018), the development of a pulsar-based time scale (Hobbs et al., 2006; Piriz et al., 2019). Downs (1974) first proposed the use of pulsar time of arrival (TOA) measurements to navigate in deep space, an application which remains an active area of research in the present day (Becker et al., 2015; Buist et al., 2011; Ely et al., 2022; Hecht et al., 2016). NASA Goddard Space Flight Center has performed a successful in-space demonstration of the use of X-ray pulsars for navigation with the Station Explorer for X-ray Timing and Navigation (SEXTANT)

experiment on-board the International Space Station (ISS) (Mitchell et al., 2018). Pulsars could also provide a source of absolute time to terrestrial users, providing timing resiliency for infrastructure applications such as power grids, communications networks, or high-frequency trading, among others (Appelquist, 2023; Financial Industry Regulatory Authority, 2016; Pini et al., 2018; United States Department of Homeland Security, 2020).

The main challenge for such a navigation system is the low signal strength of the pulsar signals, which can be as much as 50 to 60 dB below the noise floor. While pulsar observations on Earth can be conducted using large antennas such as the 100-meter diameter Green Bank Telescope at the Green Bank Observatory in West Virginia, a system designed for a spacecraft would be limited to much smaller antenna apertures due to practical size and weight constraints. When using such small apertures, due to the limited antenna gain it is necessary to perform long observations and use signal processing techniques that take advantage of the periodic nature of the signal to raise the signal-to-noise ratio (SNR) to a level at which measurements can be performed by integrating it over several hours (Heusdens et al., 2012). In general, the SNR of a radio-frequency (RF) pulsar observation is directly proportional to the effective aperture of the antenna multiplied by the square root of the total observation time. Recent studies (Jessner, 2015; Tavares et al., 2015) have suggested that a timing accuracy on the order of 1 to 10 microseconds may be feasible using an antenna with an aperture on the order of 10 square meters, taking advantage of modern computing hardware and RF components.

As previously summarized in (McKnight & van Graas, 2022) results available in the literature regarding the system performance parameters needed for a practical RF pulsar navigation system provide different outcomes. In particular, the minimum values for antenna aperture and integration time required for accurate TOA measurements are very different depending on a number of other parameters considered. A previous work (McKnight & van Graas, 2022) highlighted this gap in the requirement characterization, and noted that a terrestrial experiment could be well-suited to determine a reasonable set of system parameters and validate system performance. A follow-up work (McKnight et al., 2022) details the design and theoretical performance analysis of such an experiment and analyzes the hardware requirements of the system (Figure 1). The ultimate goal of the experiment, which will use a ~ 2 m diameter (approximately equal to a 3 m^2 aperture) dish (Figure 2) to observe pulsars, is to perform measurements of the pulsar signal and characterize the accuracy of the measurements. In this paper, the pulsar data processing and TOA measurement process is developed using simulated data, in preparation for processing real data collected by the experiment.

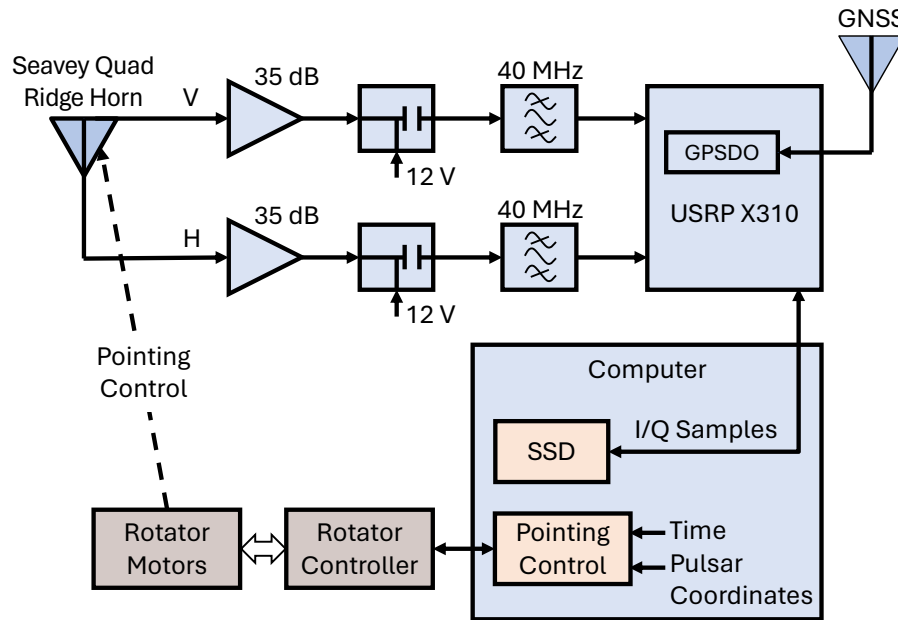


Figure 1: Block diagram of the proposed small-aperture pulsar experiment.

II. BACKGROUND

The high-level process for pulsar navigation or timing involves three steps (Winternitz et al., 2015). First, the pulsar must be observed for a total integration time t_{int} . For X-Ray pulsars, the observation involves time-tagging the arrivals of individual photons into a detector. For RF systems, the observation involves recording RF data (in-phase/quadrature (IQ) samples) and performing a process referred to as epoch folding to raise the SNR to a level at which measurements can be performed. The second step is to perform measurements, such as pulse phase or pulse frequency, using the observation data. The third and final



Figure 2: ~ 2 m diameter solid dish on a mobile platform, to be used for the proposed experiment.

step is to use the measurements as part of a timing or navigation solution, which typically involves feeding the measurements into a Kalman filter or similar estimation process. In this paper, we focus on analyzing the performance of pulse phase measurements using simulated data.

As mentioned, for RF pulsar signals it is necessary to perform epoch folding to raise the SNR of the signal to allow measurements to be performed. A graphical depiction of the process is shown in Figure 3. To begin, the observation data, which consists of a time series of samples representing power, is divided into segments numbered P_1 through P_N , where each segment is equal in duration to the pulse period of the pulsar. This requires that the pulse Doppler frequency is known to a reasonable accuracy. Next, each the individual samples in each segment are divided into a number of bins such that each segment contains the same number of bins. Typical systems use around 300 to 2000 bins per pulse period. Next, within each bin, the mean value of the samples within the bin is computed. Finally, the values in each bin are averaged across each data segment P_1 through P_N . The end result is an “integrated profile” or “folded profile” containing a number of samples equal to the number of bins, which represents the average emission of the pulsar over the span of a single pulse period during the observation. Each individual sample that is averaged reduces the variance of the noise by a factor proportional to the number of samples averaged, while the amplitude of the pulsar signal hiding below the noise is not affected. This results in an overall increase to SNR that scales as the square root of the total integration time t_{int} .

After a folded profile has been obtained, it can be used to perform a phase and frequency measurement. Typically, the measurement represents a deviation from a predicted pulse phase and frequency, where the prediction is given by a pulsar timing model. Timing models are generated by observations conducted at large observatories, such as the Green Bank Telescope, and software packages such as TEMPO2 (Hobbs et al., 2006) can predict the incoming phase and frequency of the pulse given a timing model, location, and time epoch. In this paper, we focus only on pulse phase measurement, assuming that our pulse frequency prediction is accurate enough to allow the epoch folding process to be performed (a reasonable assumption for a stationary terrestrial observer). The simplest method of phase measurement involves matched filtering, or cross-correlating the folded profile with a known replica profile (Lorimer & Kramer, 2005). While this method is conceptually simple and intuitive to understand, it is limited in resolution by the bin size in the folded profile. As an example, if pulsar B0329+54 (with a pulse period of 715 ms) is folded using 500 bins, the resolution of the cross correlation is given by 715 ms/500, or around 1.5 ms. While interpolation methods can be used to improve the resolution, there is an upper limit to precision of around 1/10 of the bin width (Lorimer & Kramer, 2005). An improved method using frequency domain techniques is given by Taylor (1992). It involves taking the discrete Fourier transform of both the folded profile and the known replica profile and minimizing a goodness-of-fit statistic formed from the Fourier coefficients of each signal as a function of the relative phase shift between the two signals. It takes advantage of the “shift property” of the Fourier transform which causes the circular time shift of a signal in the time domain to appear as a linear ramp added to the phase of the Fourier coefficients in the frequency domain. The relative phase shift between

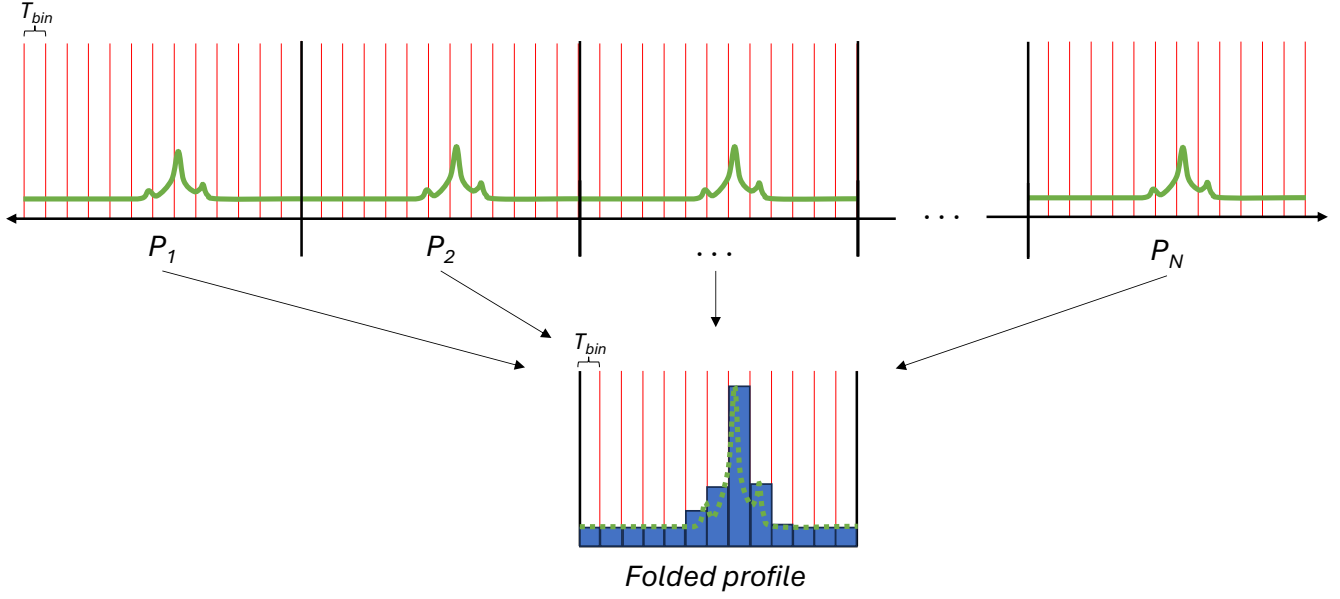


Figure 3: Illustration of the epoch folding process.

the folded profile and the replica is given by the following equation:

$$\tau = \arg \min_{\tau} \sum_{k=1}^{N/2} -P_k S_k \cos(\phi_k - \theta_k + 2\pi k\tau) \quad (1)$$

Where:

τ is the relative phase shift between the folded profile and the replica profile ($0 < \text{phase} < 1$)

$P_k e^{j\theta_k}$ are the discrete Fourier coefficients of the folded profile

$S_k e^{j\phi_k}$ are the discrete Fourier coefficients of the replica profile

N is the number of samples (number of bins) for each profile

Since the phase shift parameter τ in this method can be varied to an arbitrary precision, this method allows for timing measurements which are limited only by the SNR of the folded profile, and not by the number of bins used for folding (Wang et al., 2022). The minimization process can be performed by first conducting a coarse search over a range of values for τ , then using numerical methods such as Newton's method or Brent's method to refine the estimate.

III. SIMULATION AND RESULTS

To test and verify the pulse phase measurement process, a pulsar signal simulator was implemented using MATLAB. A block diagram for the simulation process is depicted in Figure 4.

The simulated signal is computed as the sum of the signal due to the pulsar and the signal due to system noise. The noise signal consists of band-limited (simulating a band-pass filter in the RF chain) white Gaussian noise scaled by the noise power spectral density in units of W/Hz, given by $T_{\text{sys}} k_B$, where T_{sys} is the total system noise temperature and k_B is the Boltzmann constant. Only the power of the signal ($I^2 + Q^2$) is recorded, representing a square-law detector, typically used for pulsar observations. The pulsar signal is generated by modulating a known pulse profile (normalized to mean power of 1 W/Hz) onto a "carrier" signal that is also represented by band-limited white Gaussian noise, scaled by the pulsar power spectral density in units of W/Hz, given by $S A_e$, where S is the mean pulsar flux density in units of W/m²/Hz and A_e is the effective aperture of the antenna. The use of band-limited white Gaussian noise as the "carrier" for the pulsar signal reflects the fact that the pulsar emits a wide-band signal across the entire frequency band observed. The simulation generates two channels (representing two orthogonal polarizations) of data at 100 Msps, which is the expected sample rate of the future experiment. This results in very large data

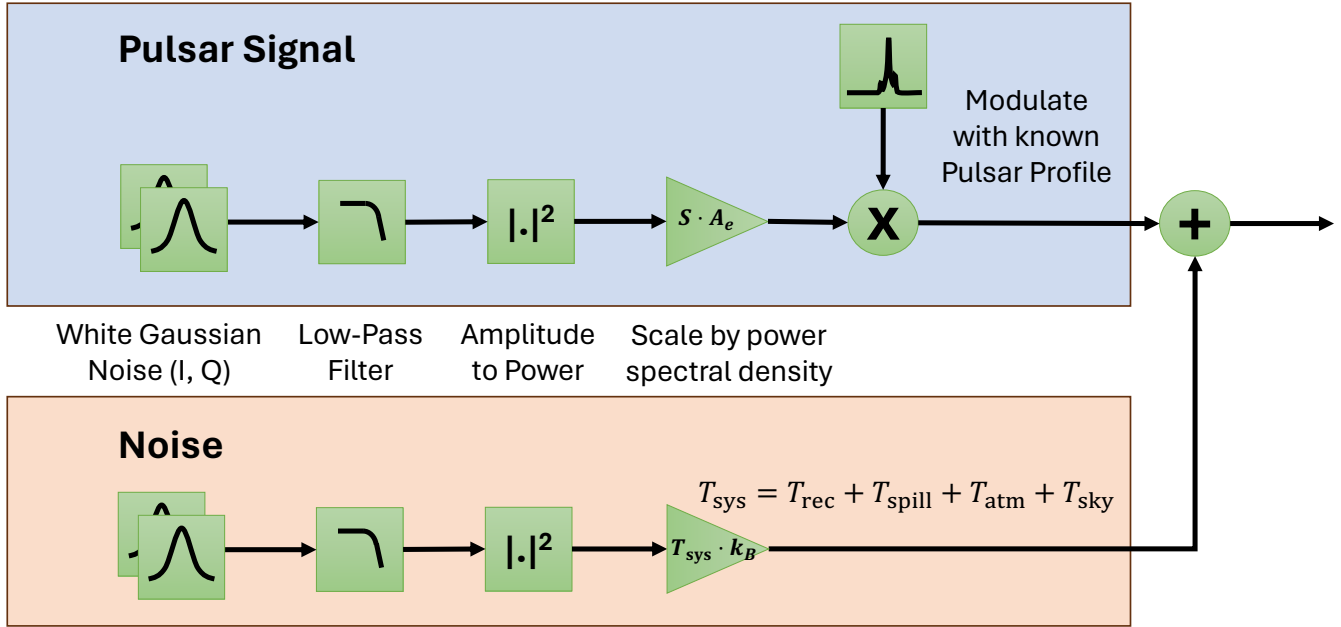


Figure 4: Block diagram of pulsar signal simulation process

rates and necessitates large run times (multiple days) to simulate 8 hours of data.

After the signal has been simulated, epoch folding is performed and the frequency domain TOA measurement technique of (Taylor, 1992) is used to estimate the phase offset of the data. The measurement is compared to the known phase offset of the simulated data to determine a timing residual. The residuals are verified by comparing them to estimations of pulsar timing accuracy available in the literature. Various expressions are available, which vary due to differing assumptions that are implicit in the models. While the expressions do not always agree with each other exactly, they typically agree within at least an order of magnitude or so. We select one such expression given by Jessner (2015):

$$\sigma_t = \frac{T_{\text{sys}}}{SG (2\pi \ln 2)^{1/4} \sqrt{\Delta f t_{\text{int}}}} \sqrt{\frac{W^3}{2P}} \quad (2)$$

Where:

σ_t is the TOA measurement error (s)

T_{sys} is the total system noise temperature (K)

S is the pulsar mean flux density (Jy)

G is the antenna gain (K/Jy)

Δf is the pre-detection bandwidth of the receiver (Hz)

τ is the post-detection integration time (s)

P is the pulse period (s)

W is the width of a single pulse (s)

Our goal is for the results of the simulation to agree with this expression to around an order of magnitude.

Multiple simulations were conducted for this study to show the effect of the system parameters on the timing residuals. In particular, the effect of the antenna effective aperture A_e , the system bandwidth Δf , and the total system noise temperature T_{sys} is analyzed. The results of these simulations are shown in Figures 5 through 13. In each row of figures, two of the parameters are held constant while one of the parameters is varied. The “reference case”, i.e. the center case in each row of figures, is the same for each row, and represents approximately the expected parameters of the planned experiment.

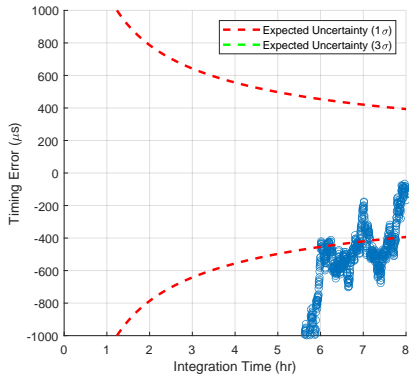


Figure 5: $A_e = 1 \text{ m}^2$, $\Delta f = 40 \text{ MHz}$,
 $T_{\text{sys}} = 100 \text{ K}$

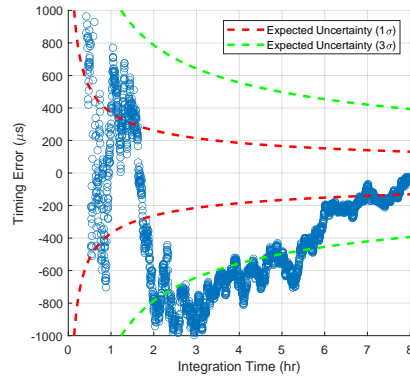


Figure 6: $A_e = 3 \text{ m}^2$, $\Delta f = 40 \text{ MHz}$,
 $T_{\text{sys}} = 100 \text{ K}$

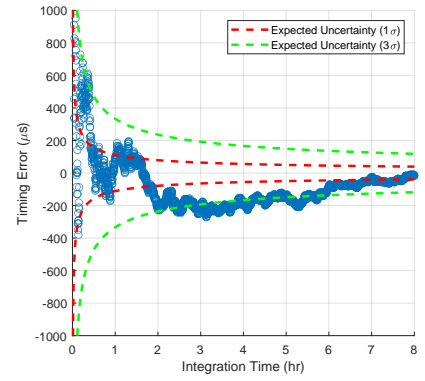


Figure 7: $A_e = 10 \text{ m}^2$, $\Delta f = 40 \text{ MHz}$,
 $T_{\text{sys}} = 100 \text{ K}$

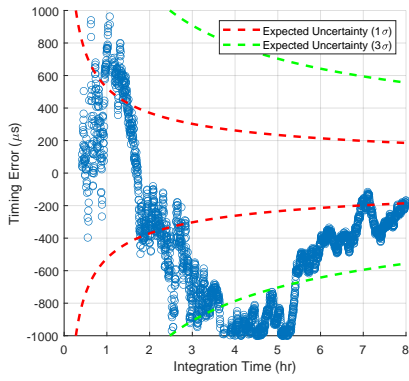


Figure 8: $A_e = 3 \text{ m}^2$, $\Delta f = 20 \text{ MHz}$,
 $T_{\text{sys}} = 100 \text{ K}$

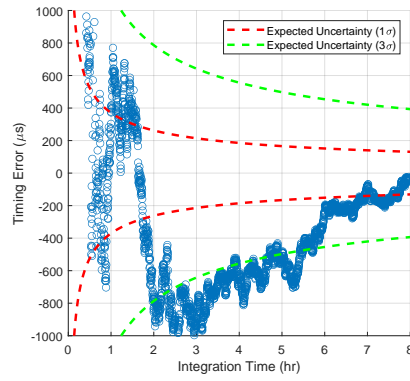


Figure 9: $A_e = 3 \text{ m}^2$, $\Delta f = 40 \text{ MHz}$,
 $T_{\text{sys}} = 100 \text{ K}$

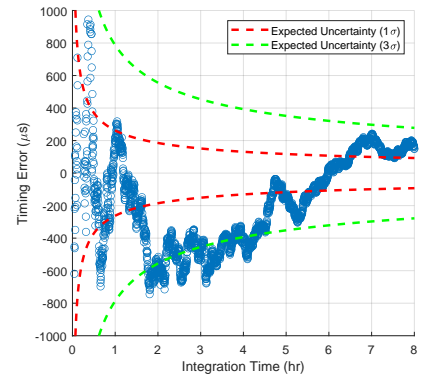


Figure 10: $A_e = 3 \text{ m}^2$, $\Delta f = 80 \text{ MHz}$,
 $T_{\text{sys}} = 100 \text{ K}$

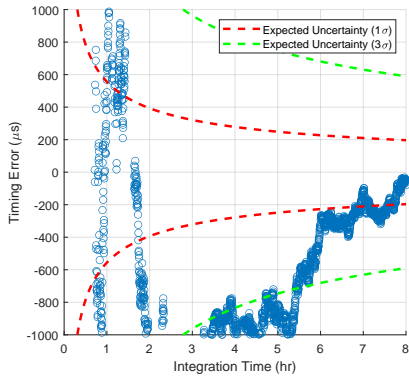


Figure 11: $A_e = 3 \text{ m}^2$, $\Delta f = 40 \text{ MHz}$,
 $T_{\text{sys}} = 150 \text{ K}$

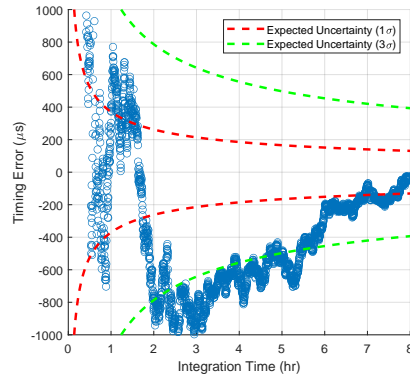


Figure 12: $A_e = 3 \text{ m}^2$, $\Delta f = 40 \text{ MHz}$,
 $T_{\text{sys}} = 100 \text{ K}$

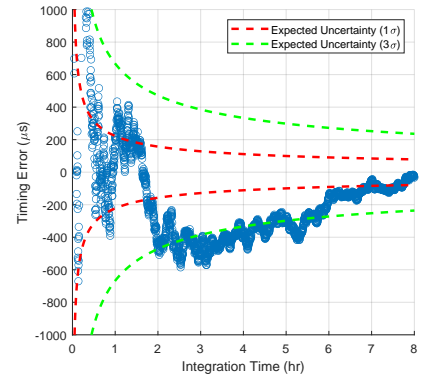


Figure 13: $A_e = 3 \text{ m}^2$, $\Delta f = 40 \text{ MHz}$,
 $T_{\text{sys}} = 60 \text{ K}$

IV. CONCLUSIONS AND FUTURE WORK

In this work, we analyzed the performance of an RF pulsar timing method using simulated data. While an interesting application of RF pulsar-based timing is related to space applications, the focus of this work was on an experiment using a stationary terrestrial observing station. The data was simulated based on the hardware design presented in previous work (McKnight et al., 2022), considering a few possible design solutions with a particular focus on a solution involving a ~ 2 m dish (approximately equal to a 3 m^2 aperture), which is the one considered for future real data collections. The data processing was implemented to perform phase measurements and retrieve the timing information by comparing the measured phase with the expected phase at the given location, based on available timing models. The simulation results given here show that the timing residuals obtained by processing simulated data agree very closely with the theoretical accuracy model given by Jessner (2015). While these simulations were used to validate and assess the method, further sets of extensive Monte Carlo simulations will be performed to bound more accurately the minimum required integration time in different settings. While here the Doppler frequency was considered to be known from the timing model, further analysis will aim to assess the effects of the frequency error, on the measurement accuracy and on the computational requirements of the system. The performance of the data processing system has been validated here with simulated data; further work will include collecting real RF data using the system shown in Figure 1 and processing it using the same techniques, allowing the simulation results to be compared to real-world measurements.

ACKNOWLEDGEMENTS

This work was supported by Ohio University.

REFERENCES

- Applequist, J. (2023). *New CIRI project to study timing requirements of 5G networks*. Retrieved August 14, 2023, from <https://ciri.illinois.edu/new-ciri-project-to-study-timing-requirements-of-5-g-networks>
- Becker, W., Bernhardt, M. G., & Jessner, A. (2015). Interplanetary GPS using pulsar signals. *Astronomische Nachrichten*, 336(8/9), 749–761. <https://doi.org/10.1002/asna.201512251>
- Becker, W., Kramer, M., & Sesana, A. (2018). Pulsar timing and its application for navigation and gravitational wave detection. *Space Science Reviews*, 214(1), 30. <https://doi.org/10.1007/s11214-017-0459-0>
- Buist, P. J., Engelen, S., Noroozi, A., Sundaramoorthy, P., Verhagen, S., & Verhoeven, C. (2011). Overview of pulsar navigation: Past, present and future trends. *NAVIGATION: Journal of The Institute of Navigation*, 58(2), 153–164. <https://doi.org/10.1002/j.2161-4296.2011.tb01798.x>
- Condon, J. J., & Ransom, S. M. (2016). *Essential radio astronomy*. Princeton University Press.
- Downs, G. S. (1974). *Interplanetary navigation using pulsating radio sources* (NASA Technical Reports No. N74-34150). Jet Propulsion Laboratory. Pasadena, California.
- Ely, T., Bhaskaran, S., Bradley, N., Lazio, T. J. W., & Martin-Mur, T. (2022). Comparison of deep space navigation using optical imaging, pulsar time-of-arrival tracking, and/or radiometric tracking. *The Journal of the Astronautical Sciences*, 69, 385–472. <https://doi.org/10.1007/s40295-021-00290-z>
- Financial Industry Regulatory Authority. (2016). *Clock synchronization* (Regulatory Notice No. 16-23). Retrieved August 15, 2023, from https://www.finra.org/sites/default/files/notice_doc_file_ref/Regulatory-Notice-16-23.pdf
- Hecht, M., Cahoy, K., Fish, V., Yoon, H., Svitek, T., & Lind, F. (2016). *A tall ship and a star to steer her by*. MIT Haystack Observatory.
- Heusdens, R., Engelen, S., Buist, P. J., Noroozi, A., Sundaramoorthy, P., Verhoeven, C., Bentum, M., & Gill, E. (2012). Match filtering approach for signal acquisition in radio-pulsar navigation. *63rd International Astronautical Congress*, 1–5.
- Hewish, A., Bell, S. J., Pilkington, J. D. H., Scott, P. F., & Collins, R. A. (1968). Observation of a rapidly pulsating radio source. *Nature*, 217, 709–713. <https://doi.org/10.1038/217709a0>
- Hobbs, G. B., Edwards, R. T., & Manchester, R. N. (2006). TEMPO2, a new pulsar-timing package – I. an overview. *Monthly Notices of the Royal Astronomical Society*, 369, 655–672. <https://doi.org/10.1111/j.1365-2966.2006.10302.x>
- Jessner, A. (2015). Technical requirements for autonomous space craft navigation using radio pulsars. *Proceedings of the 593rd WE-Heraeus Seminar on Autonomous Spacecraft Navigation*.
- Lorimer, D., & Kramer, M. (2005). *Handbook of pulsar astronomy*. Cambridge University Press.

- McKnight, R., Arnett, Z., Peters, B. C., & Ugazio, S. (2022). Performance characterization for a small-aperture radio-frequency pulsar experiment. *Proceedings of the 35th International Technical Meeting of the Satellite Division of The Institute of Navigation (ION GNSS+ 2022)*, 1933–1941. <https://doi.org/10.33012/2022.18543>
- McKnight, R., & van Graas, F. (2022). Radio-frequency pulsar observation using small-aperture antennas. *Proceedings of the 2022 International Technical Meeting of The Institute of Navigation*, 856–866. <https://doi.org/10.33012/2022.18259>
- Mitchell, J. W., Winternitz, L. B., Hassouneh, M. A., Price, S. R., Semper, S. R., Yu, W. H., Ray, P. S., Wolff, M. T., Kerr, M., Wood, K. S., Arzoumanian, Z., Gendreau, K. C., Guillemot, L., Cognard, I., & Demorest, P. (2018). SEXTANT X-Ray pulsar navigation demonstration: Initial on-orbit results [AAS 18-155]. *Proceedings of the 41st AAS Rocky Mountain Section Guidance and Control Conference (AAS/GNC 2018)*.
- Pini, M., Falletti, E., Nicola, M., Margaria, D., & Marucco, G. (2018). Dependency of power grids to satellite-derived time: Vulnerabilities and new protections. *2018 IEEE International Telecommunications Energy Conference (INTELEC)*. <https://doi.org/10.1109/INTLEC.2018.8612407>
- Píriz, R., Garbin, E., Roldán, P., Keith, M., Shaw, B., Shemar, S., Burrows, K., Davis, J., & Binda, S. (2019). PulChron: A pulsar time scale demonstration for PNT systems. *Proceedings of the 50th Annual Precise Time and Time Interval Systems and Applications Meeting*, 191–205. <https://doi.org/10.33012/2019.16753>
- Rawley, L., Stinebring, D., Taylor, J., Davis, M., & Allan, D. W. (1986). Millisecond pulsar rivals best atomic clock stability. *Proceedings of the 18th Annual Precise Time and Time Interval Systems and Applications Meeting*, 453–466.
- Shemar, S., Fraser, G., Heil, L., Hindley, D., Martindale, A., Molyneux, P., Pye, J., Warwick, R., & Lamb, A. (2016). Towards practical autonomous deep-space navigation using X-Ray pulsar timing. *Experimental Astronomy*, 42(2), 101–138. <https://doi.org/10.1007/s10686-016-9496-z>
- Tavares, G., Brito, D., & Fernandes, J. (2015). A study on the accuracy of radio pulsar navigation systems. *Proceedings of the European Navigation Conference 2015 (ENC 2015)*.
- Taylor, J. H. (1992). Pulsar timing and relativistic gravity. *Philosophical Transactions of the Royal Society of London. Series A: Physical and Engineering Sciences*, 341(1660), 117–134. <https://doi.org/10.1098/rsta.1992.0088>
- United States Department of Homeland Security. (2020). *Report on positioning, navigation, and timing (PNT) backup and complementary capabilities to the global positioning system (GPS)*. Retrieved July 23, 2023, from https://www.cisa.gov/sites/default/files/publications/report-on-pnt-backup-complementary-capabilities-to-gps_508.pdf
- Wang, J., Shaifullah, G. M., Verbiest, J. P. W., Tiburzi, C., Champion, D. J., Cognard, I., Gaikwad, M., Graikou, E., Guillemot, L., Hu, H., Karuppusamy, R., Keith, M. J., Kramer, M., Liu, Y., Lyne, A. G., Mickaliger, M. B., Stappers, B. W., & Theureau, G. (2022). A comparative analysis of pulse time-of-arrival creation methods. *Astronomy & Astrophysics*, 658, A181. <https://doi.org/10.1051/0004-6361/202141121>
- Winternitz, L. M. B., Hassouneh, M. A., Mitchell, J. W., Valdez, J. E., Price, S. R., Semper, S. R., Yu, W. H., Ray, P. S., Wood, K. S., Arzoumanian, Z., & Gendreau, K. C. (2015). X-ray pulsar navigation algorithms and testbed for SEXTANT. *2015 IEEE Aerospace Conference*. <https://doi.org/10.1109/AERO.2015.7118936>